JOURNAL OF GEOPHYSICAL RESEARCH, VOL. 86, NO. A10, PAGES 8199-8212, SEPTEMBER 30, 1981

Determination of Jupiter's Electron Density Profile From Plasma Wave Observations

D. A. GURNETT[1,2], F. L. SCARF[3], W. S. KURTH[1], R. R. SHAW[1], AND R. L. POYNTER[4]

This paper summarizes the electron density measurements obtained in the Jovian magnetosphere from the plasma wave instruments on the Voyager 1 and 2 spacecraft. Three basic techniques are discussed for determining the electron density: (1) local measurements from the low-frequency cutoff of continuum radiation, (2) local measurements from the frequency of upper hybrid resonance emissions, and (3) integral measurements from the dispersion of whistlers. The limitations and advantages of each technique are critically reviewed. In all cases the electron densities are unaffected by spacecraft charging or sheath effects, which makes these measurements of particular importance for verifying in situ plasma and low-energy charged particle measurements. In the outer regions of the dayside magnetosphere, beyond about 40 R_J, the electron densities range from about 3×10^{-3} to 3×10^{-2} cm^{-3}. On Voyager 2, several brief excursions apparently occurred into the low-density region north of the plasma sheet with densities less than 10^{-3} cm^{-3}. Approaching the planet the electron density gradually increases, with the plasma frequency extending above the frequency range of the plasma wave instrument (56 kHz, or about 38 electrons cm^{-3}) inside of about 8 R_J. Within the high-density region of the Io plasma torus, whistlers provide measurements of the north-south scale height of the plasma torus, with scale heights ranging from about 0.9 to 2.5 R_J.

1. INTRODUCTION

One of the most important parameters of a magnetospheric plasma is the electron density. The electron density occurs as a fundamental parameter in nearly all processes that occur in magnetized plasmas. Until recently the electron density in the Jovian magnetosphere was largely unknown. Several early attempts were made to estimate the plasma density distribution on the basis of theoretical models [*Gledhill*, 1967; *Ioannidis and Brice*, 1971; *Goertz*, 1973; *Michael and Sturrock*, 1974; *Mendis and Axford*, 1974]. These models revealed the importance of centrifugal stresses in the rapidly rotating magnetosphere and predicted the accumulation of plasma near the magnetic equator. The first direct measurements of plasma densities were from the Pioneer 10 and 11 plasma instrument [*Frank et al.*, 1976], which provided measurements of positive ions with energies from 100 eV to 4.8 KeV. Sensitivity limitations constrained the measurement to the inner, higher density regions of the magnetosphere. Maximum densities of about 50 to 100 protons cm^{-3} were detected at radial distances of about 2.8 R_J, in a region thought to be analogous to the plasmasphere in the earth's magnetosphere. More recently the Voyager 1 and 2 spacecraft provided much more extensive measurements of the plasma density in the Jovian magnetosphere by using a combination of charged particle intensities [*Bridge et al.*, 1979*a*, *b*; *Krimigis et al.*, 1979*a*, *b*], ultraviolet remote sensing [*Broadfoot et al.*, 1979], and radio and plasma wave phenomena [*Warwick et al.*, 1979*a*, *b*; *Scarf et al.*, 1979; *Gurnett et al.*, 1979*a*, 1980]. Among the many remarkable new results from these measurements are the observations of a dense plasma torus near the orbit of Io, with maximum electron densities of about 2000 cm^{-3} at about 5.8 R_J, the observations of a very hot $\sim 3 \times 10^8$ °K plasma boundary layer (magnetospheric wind) between the outer magnetosphere and the solar wind, and the observations of regions of extremely low electron density, $\sim 10^{-5}$ to 10^{-6} cm^{-3}, in the distant tail lobe.

Since many of the new Voyager electron density determinations rely on the interpretation of plasma wave measurements, the purpose of this paper is to review critically the techniques employed and to present the latest results by using all of the data currently available. Three basic techniques for determining the electron density will be discussed: (1) local measurements from the low-frequency cutoff of continuum radiation, (2) local measurements from the frequency of upper hybrid resonance emissions, and (3) integral measurements from the dispersion of whistlers. As will be discussed, each of these techniques provides unique advantages in different regions of the magnetosphere. In all cases the electron density determinations are believed to be unaffected by spacecraft charging or sheath effects, since the electron density is determined directly from a characteristic frequency or dispersion property of the plasma averaged over spatial scales much larger than the spacecraft. The plasma wave electron density measurements should therefore be extremely accurate and reliable. The results are therefore presented in a format intended to be useful not only for an overview of the plasma density distribution in the Jovian magnetosphere, but also for cross comparison with other instruments in cases where good accuracy and precise knowledge of the local electron density are important.

2. ELECTRON DENSITIES FROM THE CONTINUUM RADIATION CUTOFF

Measurements of the electron density from the low-frequency cutoff of continuum radiation are based on an effect first observed at the earth by *Gurnett and Shaw* [1973] in which electromagnetic radiation is observed to be trapped in the earth's magnetosphere at frequencies above the electron plasma frequency f_p. As is well known [*Stix*, 1962], the elec-

[1] Department of Physics and Astronomy, The University of Iowa, Iowa City, Iowa 52242.
[2] Research performed while on leave at the Institute of Geophysics and Planetary Physics, University of California, Los Angeles, California 90024.
[3] Space Sciences Department, TRW Defense and Space Systems Group, Redondo Beach, California 90278.
[4] Jet Propulsion Laboratory, Pasadena, California 91103.

Paper number 80A1281.
0148-0227/81/080A-1281$01.00

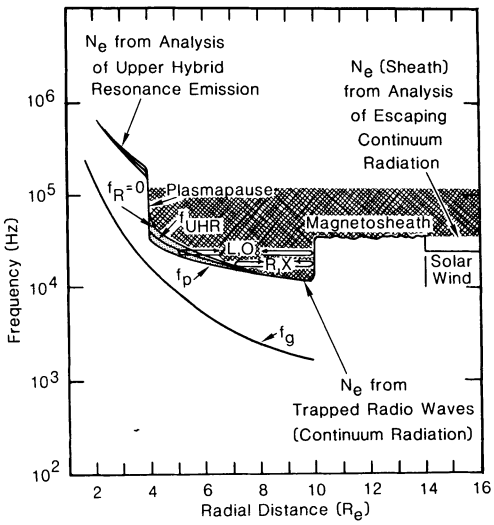

Fig. 1. A typical radial profile of the critical frequencies of the plasma in the earth's magnetosphere showing the reflection and trapping of radio waves at frequencies above the electron plasma frequency f_p.

tron plasma frequency is the lowest frequency at which the free space electromagnetic mode can propagate. Because reflection occurs at the plasma frequency, electromagnetic radiation can be trapped in the low-density regions between the plasmapause and magnetopause as illustrated in Figure 1. The low-frequency cutoff of the trapped radiation can therefore be used to determine the electron density from the local plasma frequency $f_p = 9\sqrt{N_e}$ kHz, where N_e is the electron density in cm^{-3}. Because the spectrum of the radiation trapped in the earth's magnetosphere is essentially continous in both frequency and time, this radiation has been called continuum radiation [*Gurnett,* 1975]. Recently, the same type of radiation has been observed in the Jovian magnetosphere [*Scarf et al.,* 1979; *Gurnett et al.,* 1979*a*]. Although the origin of the radiation has not been completely established, two basic mechanisms have been proposed. One possibility is that the radiation is gyrosynchrotron radiation from energetic electrons [*Frankel,* 1973]. The other and currently favored mechanism is that the radiation is generated by coupling with electrostatic waves near the upper hybrid resonance frequency [*Gurnett,* 1975; *Gurnett and Frank,* 1976; *Jones,* 1976; *Christiansen et al.,* 1978; *Kurth et al.,* 1979]. The electrostatic wave coupling mechanism has recently been given substantial theoretical support by *Melrose* [1981].

An example of the continuum radiation observed at Jupiter is illustrated in Figure 2, which shows the first magnetopause crossing by Voyager 1. The upper panel shows the electric field intensities in eleven frequency channels from 178 Hz to 56.2 kHz for a 4-hour interval centered on the magnetopause crossing, and the bottom panel shows a high-resolution frequency-time spectrogram of 96 s of wideband waveform data obtained around 2036 UT (all times are spacecraft event times). For a description of the instrumentation used to obtain these data, see *Scarf and Gurnett* [1977]. The sharp cutoff of the continuum radiation as the spacecraft enters the low-density region of the outer magnetosphere is clearly evident in Figure 2. A dashed line showing the approximate variations in the low-frequency cutoff of the continuum radiation is shown in the top panel. The high-resolution spectrogram in the bottom panel shows that the cutoff is extremely sharp, very similar to the cutoff observed for the earth's trapped continuum

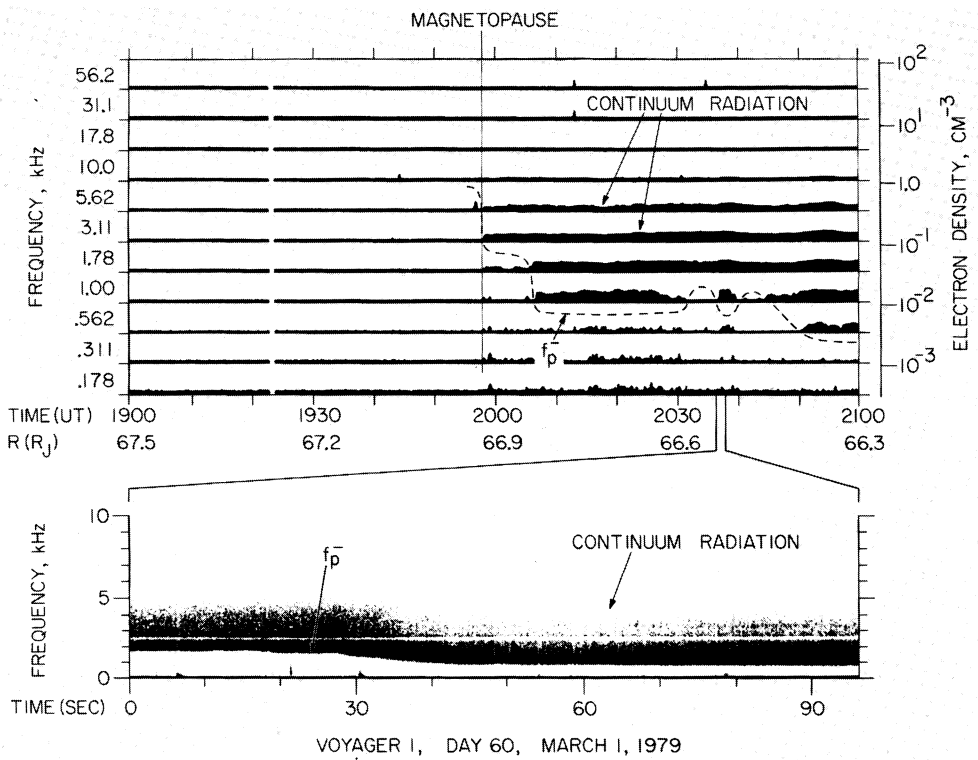

Fig. 2. The Voyager 1 entry into the Jovian magnetosphere showing the occurrence of continuum radiation trapped in the magnetosphere. The low-frequency cutoff of the continuum radiation is at the electron plasma frequency, which gives the electron density as shown by the scale to the right of the top panel. Brief bursts of wideband data, as shown in the bottom panel, provide very high resolution measurements of the electron density.

TABLE 1. Electron Densities From Voyager 1 Wideband Measurements of Continuum Radiation

Date	SCET	f_{MAX}, Hz	f_{MIN}, Hz	N_{MAX}, cm^{-3}	N_{MIN}, cm^{-3}	R, R_J
March 1, 1979	2033:24	1750	1820	3.78×10^{-2}	4.09×10^{-2}	66.5
	2034:12	1820	1700	4.29×10^{-2}	3.57×10^{-2}	66.5
	2036:36	1650	900	3.36×10^{-2}	1.00×10^{-2}	66.5
	2037:24	900	750	1.00×10^{-2}	6.94×10^{-3}	66.4
	2039:48	1275	1350	2.01×10^{-2}	2.25×10^{-2}	66.4
	2940:36	1350	1150	2.25×10^{-2}	1.63×10^{-2}	66.4
March 4, 1979	1343:46	6100	5900	4.59×10^{-1}	4.30×10^{-2}	21.3

*The frequency variation over each 48-s frame is characterized by tabulating the maximum and minimum cutoff frequency. The maximum and minimum density values represent the variability over the 48-s interval.

radiation. On the basis of the close similarity to the terrestrial continuum radiation, this cutoff is identified as the local electron plasma frequency. A corresponding electron density scale is shown to the left of the top panel. As can be seen the electron densities in the outer magnetosphere range from about 3 $\times 10^{-3}$ cm^{-3} to 3 $\times 10^{-2}$ cm^{-3}. These electron densities are in good quantitative agreement with the densities reported by *Scudder et al.* [this issue] using measurements from the Voyager plasma instrument.

It is useful now to consider the uncertainties that can arise in determining the electron density from the continuum radiation cutoff. First, as illustrated in Figure 1, two propagation cutoffs occur for the free space modes; one at f_p for the left-hand polarized ordinary (L, O) mode and the other at a slightly higher frequency, $f_{R=0} = f_g/2 + \sqrt{(f_g/2)^2 + f_p^2}$, for the right-hand polarized (R, X) mode, where f_g is the electron gyrofrequency. Either of these cutoffs could in principle be responsible for the continuum radiation cutoff. However, in the earth's magnetosphere, and presumably also at Jupiter, the trapped continuum radiation consists of both right-hand and left-hand polarized waves with approximately equal intensities [*Gurnett and Shaw,* 1973]. Since some left-hand polarized waves are always present, the lowest propagation cutoff always corresponds to the electron plasma frequency. Second, although the electron plasma frequency is the proper cutoff for the mode involved, there is no guarantee that this cutoff actually corresponds to the local electron plasma frequency. For example, the observed cutoff could correspond to the plasma frequency cutoff at some remote point between the source and the observer. In fact, the only firm conclusion that can be made in all cases is that the observed cutoff gives an upper limit to the local plasma frequency. Despite this weakness, it is our conclusion from studies of the terrestrial continuum radiation [*Gurnett and Frank,* 1974; *Shaw and Gurnett,* 1975, 1980] that the continuum radiation cutoff can be used to provide accurate measurements of the local electron plasma frequency. The principal indicator of the local nature of the propagation cutoff is the sharpness of the cutoff. If the propagation cutoff is very sharp it is our experience from terrestrial observations that the cutoff always corresponds to the local electron plasma frequency. A sharp cutoff is produced whenever a broad frequency spectrum of noise propagates into a region of increasing plasma density, thereby producing a cutoff that depends on the plasma frequency at the observing point. The increasing electron density with decreasing radial distance in the outer magnetospheres of both Jupiter and the earth provides favorable geometries for producing a sharp cutoff of reflected continuum radiation at the local electron plasma frequency. In some regions of the earth's magnetosphere, such as in the distant geomagnetic tail, the continuum radiation spectrum does not extend down to the local propagation cutoff. In these regions the cutoff is not sharp and does not correspond to the local plasma frequency. Similar effects also appear to occur in the low-density tail lobe regions of the Jovian magnetosphere [*Gurnett et al.,* 1980].

Two characteristics of the continuum radiation are necessary to account for the local nature of the propagation cutoff. One is that the source must have a broad bandwidth with frequencies extending down to the local electron plasma frequency, and the other is that the waves must have a nearly isotropic angular distribution. At both Jupiter and the earth the continuum radiation is observed to have a very broad bandwidth extending down to the local plasma frequency throughout a wide region of the outer magnetosphere. The reason for the broad bandwidth of the emission is not completely understood. If the source is gyrosynchrotron radiation, as proposed by *Frankel* [1973], then a broadband emission extending down to the local plasma frequency would be expected. On the other hand, coupling from electrostatic waves would not provide a broadband spectrum since the electrostatic waves tend to produce narrow band emissions from isolated regions near the magnetic equator [*Kurth et al.,* 1980]. Recently, however, *Barbosa* [1980] has suggested an inverse Compton scattering mechanism that may be able to explain the spreading of trapped continuum radiation spectrum down to the local propagation cutoff.

For the continuum radiation cutoff to correspond to the local electron plasma frequency it is also essential that at least some of the waves be incident normal to the constant density surface. Otherwise, reflection will occur at a frequency above the local plasma frequency. This requirement appears to be satisfied for continuum radiation trapped in the earth's magnetosphere, since the electric field distribution (hence wave vector distribution) is very nearly isotropic [*Gurnett,* 1975]. The isotropic angular distribution probably arises because of the large number of complex reflections that take place within the magnetospheric cavity. Since the trapping process is presumably the same in the Jovian magnetosphere, the angular distribution is also expected to be isotropic at Jupiter.

In addition to the above basic considerations, other instrumentational limitations also affect the accuracy and interpretation of the electron density measurements. As illustrated in Figure 2, two different types of spectrum measurements are available from the Voyager plasma wave instrument. The 16-channel electric field intensity measurements shown in the top panel provide essentially continuous survey measurements with relatively coarse frequency resolution. With these data the electron density can only be determined within a factor of three. Much better resolution can be obtained from wideband spectrum measurements such as in the bottom panel of Figure

TABLE 2. Electron Densities From Voyager 2 Wideband Measurements of Continuum Radiation

Date	SCET Time	f_{MAX}, Hz	f_{MIN}, Hz	N_{MAX}, cm^{-3}	N_{MIN}, cm^{-3}	R, R_J
July 5, 1979	0003:59	5000	3750	3.10×10^{-1}	1.74×10^{-1}	71.4
	0004:47	4050	2250	2.02×10^{-1}	6.25×10^{-2}	71.4
	0005:35	2750	2550	9.34×10^{-2}	8.03×10^{-2}	71.4
	0006:23	2600	2250	8.34×10^{-2}	6.25×10^{-2}	71.4
	0058:23	5850	3150	4.23×10^{-1}	1.23×10^{-1}	71.0
	0059:11	3100	2200	1.19×10^{-1}	6.00×10^{-2}	70.9
	0059:59	2400	2100	7.11×10^{-2}	5.44×10^{-2}	70.9
	0100:47	2700	2150	9.00×10^{-2}	5.71×10^{-2}	70.9
	2159:59	706	706	6.15×10^{-3}	6.15×10^{-3}	60.2
	2200:47	753	706	7.00×10^{-3}	6.15×10^{-3}	60.2
July 6, 1974	1110:23	800	700	7.90×10^{-3}	6.05×10^{-3}	53.3
	1111:11	800	700	7.90×10^{-3}	6.05×10^{-3}	53.3
	1117:35	850	750	8.92×10^{-3}	6.94×10^{-3}	53.2
	1118:23	800	750	7.90×10^{-3}	6.94×10^{-3}	53.2
	1222:23	850	800	8.92×10^{-3}	7.90×10^{-3}	52.7
	1357:35	1150	1100	1.63×10^{-2}	1.49×10^{-2}	51.8
	1535:11	700	700	6.05×10^{-3}	6.05×10^{-3}	51.0
	1603:59	850	800	8.92×10^{-3}	7.90×10^{-3}	50.7
	1755:11	850	700	8.92×10^{-3}	6.05×10^{-3}	49.7
	1800:47	800	700	7.90×10^{-3}	6.05×10^{-3}	49.7
	1901:35	1100	950	1.23×10^{-2}	1.11×10^{-2}	49.1
	2211:11	1200	1100	1.78×10^{-2}	1.49×10^{-2}	47.4
July 7, 1974	0136:47	979	978	1.18×10^{-2}	1.18×10^{-2}	45.6
	1059:59	950	700	1.11×10^{-2}	6.05×10^{-3}	40.4
	1105:35	850	700	8.92×10^{-3}	6.05×10^{-3}	40.3
	1158:23	1150	1000	1.63×10^{-2}	1.23×10^{-2}	39.9
	1411:59	1750	1250	3.78×10^{-2}	1.93×10^{-2}	38.6
	1638:23	1850	1700	4.22×10^{-2}	3.57×10^{-2}	37.3
	1802:23	1630	1630	3.28×10^{-2}	3.28×10^{-2}	36.5

The frequency variation over each 48-s frame is characterized by tabulating the maximum and minimum cutoff frequency. The maximum and minimum density values also represent the variability over the 48-s interval.

2. Typically, the electron density can be obtained from the wideband data with an accuracy of a few percent. Unfortunately, because the wideband data transmission must be shared with the imaging system, wideband high-resolution spectrums can only be obtained for a limited number of 48-s frames scattered throughout the encounter. During the pass through the magnetosphere, a total of 10,497 frames of wideband data were obtained from Voyager 1, and 1,574 frames were obtained from Voyager 2 [*Scarf et al.*, this issue]. Of these, only a small number, 301 frames from Voyager 1 and 81 frames from Voyager 2, are currently available for analysis.

Since the highest resolution and best accuracy are obtained from the wideband data, the primary emphasis in this paper will be on the electron densities obtained from the wideband spectrograms. Complete listings of the continuum radiation cutoffs obtained from all of the wideband data currently available for analysis are given in Tables 1 and 2. Each time listed represents the start time for a 48-s frame of wideband data. Since the plasma density often changes substantially over periods of only a few seconds, the maximum and minimum cutoff frequencies, f_{max} and f_{min}, and the associated maximum and minimum electron density, N_{max} and N_{min}, are given for each time interval. The very rapid temporal variations that are sometimes observed are illustrated in Figure 3, which shows a sequence of high-resolution spectrum measurements from Voyager 2 during the interval from 0058:54 to 0059:28 UT on July 5, 1979. The very sharp low-frequency cutoff, characteristic of the continuum radiation, is clearly evident in the three amplitude spectrums shown at the top of the illustration. Careful measurements indicate that the continuum radiation intensity decreases by as much as 20 db in a frequency range of only 100 Hz near the cutoff. In cases such as this the instantaneous electron density can be determined with an accuracy of about 1–2% on a time scale of only 0.1 s. As can be seen, very large density changes, as much as a factor of four, can occur in a time of only 10 s. Although this case illustrates an extreme example of time variability, inspection of Tables 1 and 2 shows that electron density variations of 10–30% are not uncommon during any given 48-s interval. These variations in the plasma density must be considered when comparisons are made with other instruments that have time resolutions longer than the time scale of the fluctuations. The high resolution spectrums in Figure 3 also show the occurrence of several narrowband enhancements in the continuum radiation spectrum. Narrowband features of this type are occasionally observed in both the terrestrial and Jovian continuum radiation spectrum and are suggestive of discrete narrowband sources for the continuum radiation, as would be expected for the electrostatic wave coupling mechanism. The fairly well defined upper cutoff in the spectrum at about 6.5 kHz may represent the transition from the trapped to the escaping regions as illustrated in Figure 1. An abrupt decrease in the trapped continuum radiation intensity is expected at this transition because of the intensity enhancement provided by repeated reflections of the radiation within the magnetosphere.

The electron density profiles obtained from the 16-channel spectrum analyzer survey data during the inbound passes of Voyager 1 and 2 are shown in Figures 4, 5, and 6. The corresponding outbound passes through the tail of the magnetosphere have been previously published and analyzed by *Gurnett et al.* [1980]. Combined plots of both the peak and average intensities and the average intensity alone are shown. Since the continuum radiation is relatively steady, the low-frequency cutoff is most clearly identified in the average in-

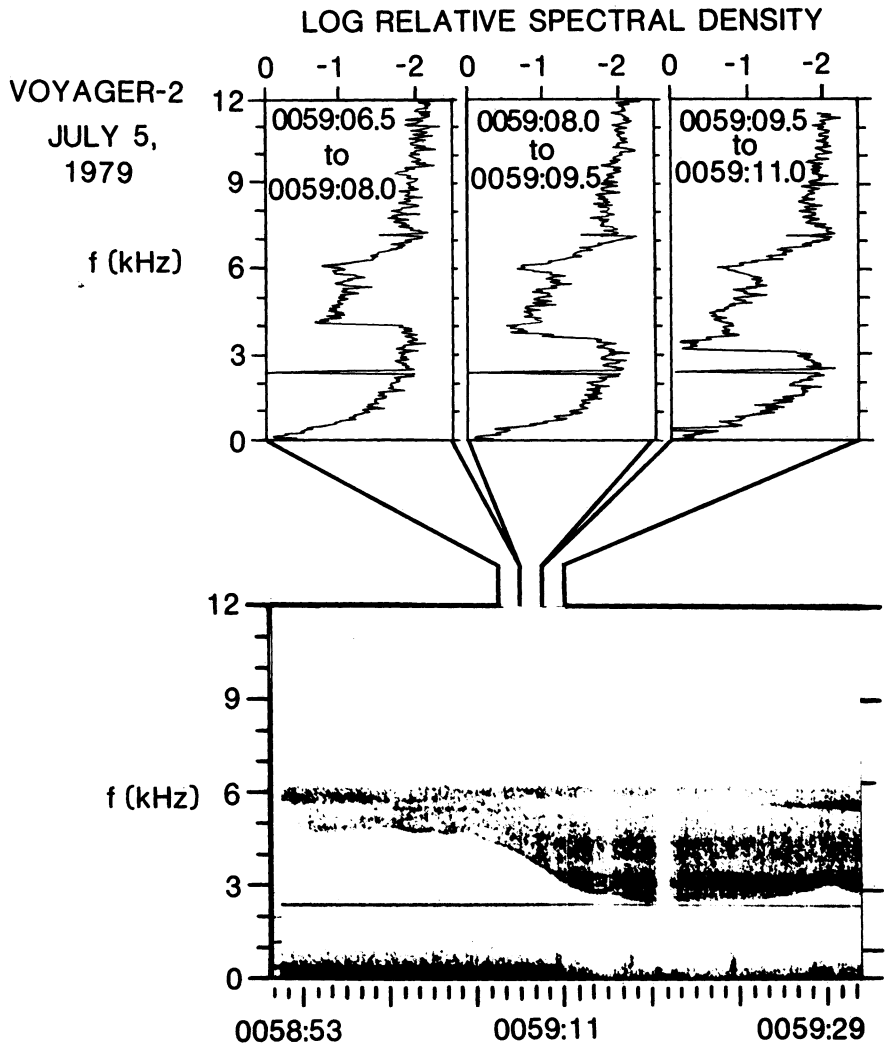

Fig. 3. A sequence of very high resolution spectrums of wideband data showing the extremely sharp low-frequency cutoff and rapid changes in the electron density that sometimes occur in the outer regions of the magnetosphere.

tensities. The best estimate of the cutoff frequency, hence electron density, is shown by the solid line. As was previously discussed, the electron density obtained from the survey data is uncertain by about a factor of 3 because of the basic frequency spacing between the channels. Also, the electron density line on these plots does not attempt to follow electron density variations on time scales less than about one half hour because of the very compressed time scale. For comparison, the more accurate electron densities obtained from the wideband measurements listed in Tables 1 and 2 are shown by the solid circles.

As can be seen from a comparison of the electron density profiles in Figures 4, 5, and 6, the structure of the outer magnetosphere was quite different on the inbound passes of Voyager 1 and 2. For Voyager 1 the final entry into the magnetosphere occurred much closer to the planet than for Voyager 2, 46.7 versus 61.9 R_J, indicating a more compressed magnetosphere. The average electron densities in the outer magnetosphere are somewhat higher for Voyager 1, $\sim 3 \times 10^{-2}$ cm^{-2}, compared with $\sim 1 \times 10^{-2}$ cm^{-3} for Voyager 2. Approaching the planet, the electron density gradually increases until the continuum radiation cutoff can no longer be clearly identified inside of about 20 R_J. Contrary to our earlier report on the magnetotail densities [*Gurnett et al.*, 1980], several very brief regions can now be identified in which Voyager 2 apparently entered regions of extremely low density, less than 10^{-3} cm^{-3}, on the dayside of Jupiter, comparable to the extremely low densities observed in the tail lobe on the nightside of Jupiter. These low density regions are evident from about 1120 to 1150 on July 7, and from about 0230 to 0430 UT, 1000 to 1100 UT, and 1310 to 1430 UT on July 8 in Figure 6. All of these low density regions occur when the spacecraft is near the maximum north magnetic latitude, apparently representing crossings of the northern boundary of the dayside plasma sheet. No comparable dayside low-density regions were detected by Voyager 1, probably because Voyager 1 approached Jupiter at a slightly lower latitude than Voyager 2; approximately 3.1° versus 7.2°. It is also interesting to note that the entries into the very low density region occurred relatively close to the planet (~25 to 40 R_J) and not in the outer regions of the magnetosphere. This relationship is an almost exact parallel to the nightside electron density observations in which the entry into the low-density tail lobe region was confined to an intermediate range of radial distances between the inner magnetosphere and the latitudinally extended plasma boundary layer found near the outer boundary of the magnetosphere. These observations of comparable electron density distributions on the dayside and nightside of the magnetosphere now provide

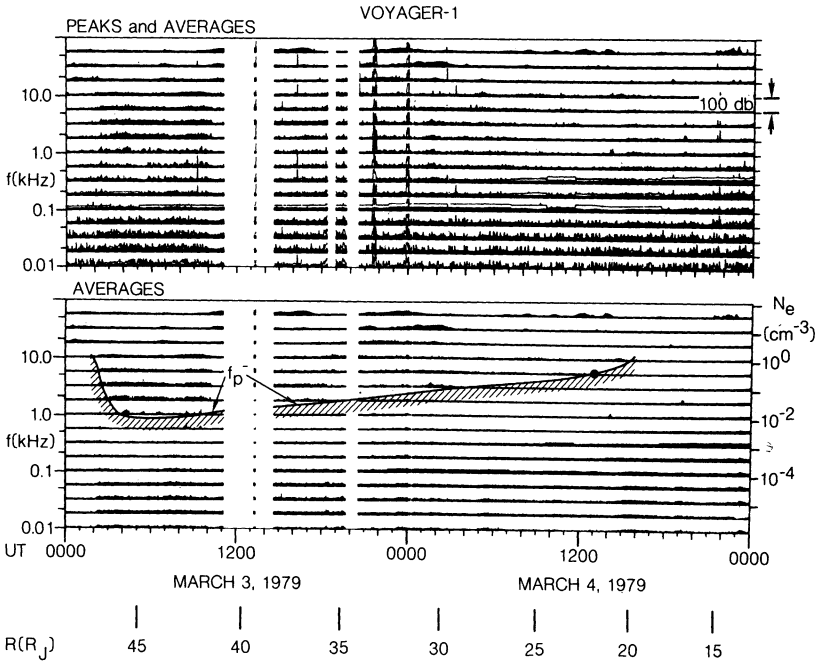

Fig. 4. The continuum radiation and electron density profile (dashed line) obtained for the inbound pass of Voyager 1. Only one burst of wideband data is available for high-resolution electron density measurements during this period. The electron density from the wideband data is shown by the solid black dot.

strong evidence that the plasma boundary layer found on the nightside of Jupiter extends around into the dayside of the magnetosphere. The electron densities in both the nightside [see *Gurnett et al.,* 1980] and dayside plasma boundary layer regions are quite similar, $\sim 3 \times 10^{-3}$ cm^{-3} to 1×10^{-2} cm^{-3}, with slightly higher densities occurring on the dayside of the magnetosphere.

3. Electron Densities From Upper Hybrid Resonance Emissions

Electrostatic emission associated with the local upper hybrid resonance frequency, $f_{UHR} = \sqrt{f_p^2 + f_g^2}$, has been observed for many years by rocket-borne and satellite-borne plasma wave instruments [*Walsh et al.,* 1964; *Hartz,* 1970; *Mosier et al.,* 1973; *Shaw and Gurnett,* 1975; *Hubbard and Birmingham,* 1978; *Rönnmark et al.,* 1978; *Christiansen et al.,* 1978; *Kurth et al.,* 1979]. Although the details of these emissions vary somewhat in different regions of the magnetosphere, the common feature is that an intense electrostatic emission is observed near the local upper hybrid resonance frequency. Since the upper hybrid resonance frequency depends on the electron plasma frequency, a measurement of the emission frequency and knowledge of the magnetic field strength (to give f_g) provide a determination of the electron density. For the special case when $f_p \gg f_g$, which is frequently encountered in magnetospheric plasmas, the upper hybrid resonance frequency is essentially coincident with the electron plasma frequency (see Figure 1).

At least two mechanisms are known to be involved in the generation of the upper hybrid resonance emissions: (1) Cerenkov radiation by energetic electrons, and (2) instabilities driven by velocity space anisotropies in the electron distribution function. At Jupiter the upper hybrid resonance (UHR) emissions are all believed to be of the latter type. The basic instability that produces the upper-hybrid resonance emissions is closely associated with a class of instabilities that occur near half-integral harmonics of the electron gyrofrequency, $(n + 1/2)f_g$. In an inhomogeneous plasma the upper hybrid resonance emissions do not occur as a single continuous emission at f_{UHR}, but rather as a discontinuous series of emission lines whenever $f_{UHR} \simeq (n + 1/2)f_g$. The discontinuous discrete character of the UHR emissions has been observed at both the earth [*Kurth et al.,* 1979] and Jupiter [*Gurnett et al.,* 1979*a*], and now has a reasonably well-developed theoretical basis [*Hubbard and Birmingham,* 1978; *Ashour-Abdalla et al.,* 1979]. An example of the UHR emissions detected by Voyager 2 at Jupiter that illustrates the discontinuous character of the emission frequency is shown in Figure 7. The frequency spacing between the bands is approximately the electron gyrofrequency. Because of the quantified character of the

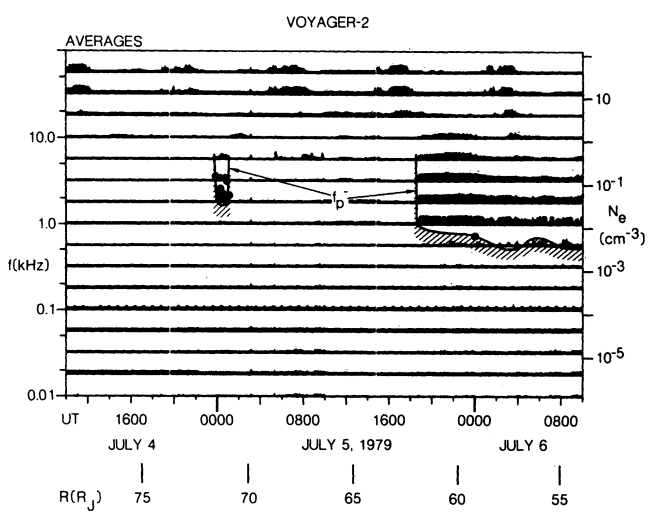

Fig. 5. The continuum radiation and electron density profile (dashed line) for the inbound pass of Voyager 2. The electron densities in the outer regions of the magnetosphere are typically about 10^{-2} cm^{-3}.

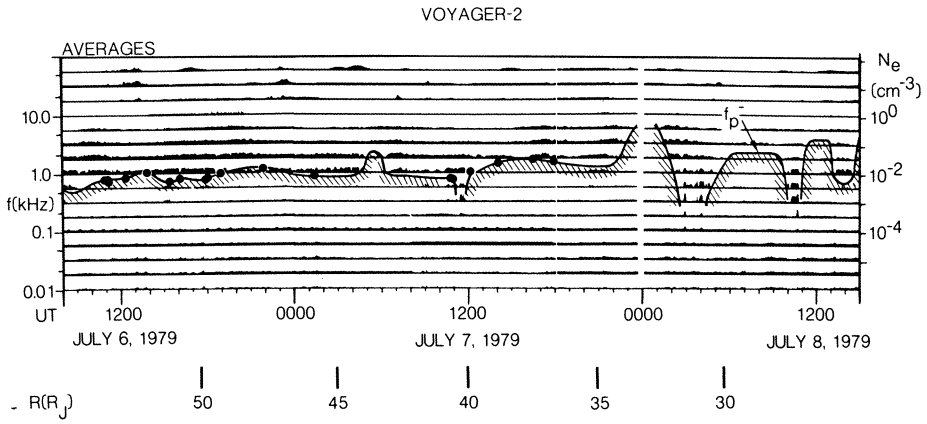

Fig. 6. A continuation of Figure 5 for the inner portion of the Voyager 2 pass. In addition to a general rise in the plasma density as the spacecraft approaches the planet, several abrupt 'dropouts' in the plasma density occur, at ~1135 UT on July 7 and ~0330, 1030, and 1350 UT on July 8. These regions are similar to the regions of extremely low density observed in the lobes of the Jovian magnetotail and probably represent crossings into a very low density region above the plasma sheet.

emission frequency, the accuracy with which the electron density can be determined is inherently limited by the band spacing, which is approximately f_g. For the special case when $f_p \gg f_g$, the fractional uncertainty in the electron density is approximately $\Delta N/N \simeq 2(f_g/f_p)$. For representative terrestrial and Jovian plasma parameters, this uncertainty usually limits the accuracy of the electron density determination to a few percent, although as f_g/f_p increases, the uncertainty can become much larger. Another factor that must be considered in the interpretation has to do with the relative contribution of cold and hot electrons to the total density. Although the exact instability conditions depend in a complicated way on the cold and hot densities [see *Hubbard and Birmingham,* 1978; *Ashour-Abdalla et al.,* 1979], the emission frequency is mainly controlled by the upper hybrid resonance frequency of the cold electrons. Thus, in contrast to the continuum radiation cutoff, which is insensitive to the plasma temperature (provided the plasma is not relativistic), the electron density determined by the upper hybrid resonance frequency is mainly characteristic of the cold ≲100-eV electrons. In most cases, however, the density of the hot electrons is only a small fraction of the total electron density, so the upper hybrid resonance still provides a good estimate of the total electron density. In all cases where comparisons between the continuum radiation cutoff and UHR emission frequency have been possible, the electron densities obtained from the two techniques are in good agreement. Figure 7, for example, shows a case where the continuum radiation cutoff is almost coincident with the frequency of the UHR emissions, as expected when $f_g \ll f_p$.

At Jupiter, upper hybrid resonance emissions are observed primarily at radial distances inside of 25 R_J. The electron density measurements from UHR emissions therefore nicely complement the continuum radiation measurements since the con-

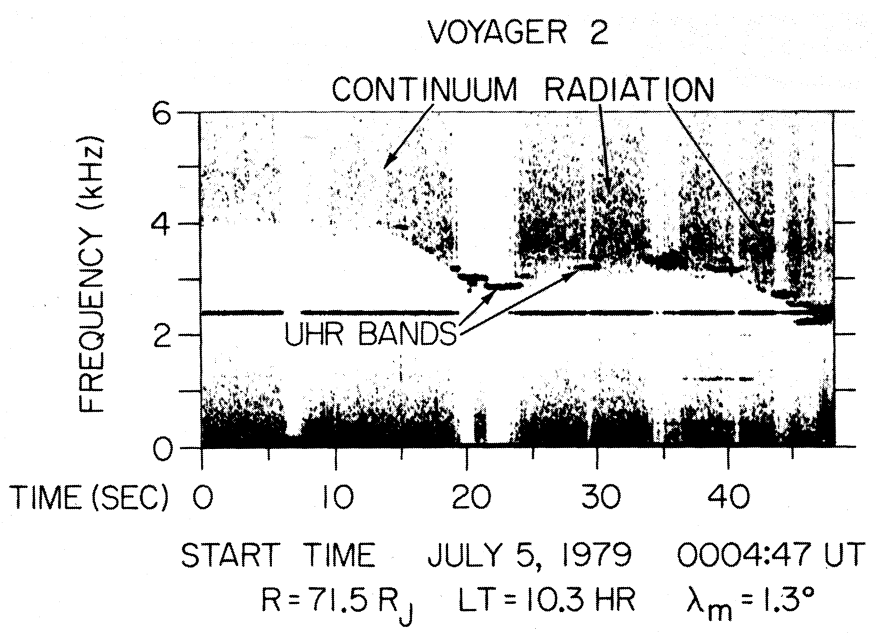

Fig. 7. A wideband spectrogram showing the occurrence of intense emissions at the upper hybrid resonance (UHR) frequency. Note the discontinuous character of the emission, which only occurs if $(n + 1/2)f_g \simeq f_{UHR}$. The UHR emissions occur very close to the low-frequency cutoff of the continuum radiation, as expected since $f_{UHR} \simeq f_p$ when $f_g \ll f_p$.

TABLE 3. Electron Densities From Upper Hybrid Resonance Emissions

Spacecraft	Date	SCET	f_{UHR}, kHz	N, cm^{-3}	Identification	R, R_J
Voyager 1	March 4, 1979	1825	17.8	2.9–5.2	Good	17.6
	March 5, 1979	0010	31.1	8.9–16	Excellent	13.0
	March 6, 1979	0450	17.8	2.9–5.2	Poor	16.8
	March 6, 1979	1630	3.1	0.089–0.16	Poor	25.9
Voyager 2	July 9, 1979	0940	31.1	8.9–16	Poor	13.9
	July 9, 1979	1330	56.2	29–52	Good	12.2
	July 9, 1979	2215	56.2	29–52	Excellent	10.1
	July 10, 1979	0010	56.2	29–52	Excellent	10.2
	July 10, 1979	0910	31.1	8.9–16	Excellent	13.0
	July 10, 1979	1220	17.8	2.9–5.2	Excellent	14.5
	July 10, 1979	1915	10.0	0.92–1.6	Poor	18.3

Identifications are ranked according to the certainty with which the event can be identified as a UHR emission. Error limits correspond to one quarter channel spacing.

tinuum radiation is usually too weak to be detected inside of 25 R_J. Unfortunately, the UHR emissions also tend to be confined to the magnetic equator [*Kurth et al.*, 1980], so that electron density measurements are normally possible only when the spacecraft is crossing the magnetic equator. An exception to this rule apparently occurs in the Io plasma torus, where the radio astronomy instrument [*Warwick et al.*, 1979*a*] detected UHR emissions well away from the magnetic equator. A summary of all of the electron density measurements obtained from the upper hybrid resonance technique is given in Table 3, and the corresponding points are plotted in Figures 8 and 9. For the Voyager 1 pass in Figure 8, only four clearly defined UHR events can be identified in the plasma wave data. These four events are shown circled in the second panel from the top in Figure 8. The event at 0010 UT on March 5 is very intense and occurs exactly at the magnetic equator crossing. This event occurs well above the emissions at $(3/2)f_g$ and $(5/2)f_g$ and is almost certainly a UHR emission. The corresponding electron density is shown by the solid black dot in the top panel. The events at 1800 UT on March 4 and at 0530 and 1630 UT on March 6 are very weak and do not occur precisely at the magnetic equator crossing. Because the identification of these three events as UHR emissions is more uncertain, the corresponding electron density points are shown as open circles in the top panel. Inside of about 8 R_J the electron density is so large that the upper hybrid resonance frequency extends above the frequency range of the plasma wave instrument and into the range of the radio astronomy instrument. In this region an extensive series of UHR emissions occurred that allowed the radio astronomy team to provide a nearly continuous electron density profile through the Io plasma torus [*Warwick et al.*, 1979*a*]. The electron densities from the radio astronomy instrument are shown at the top of Figure 8 [from *Birmingham et al.*, this issue] and are connected to the plasma wave measurements by a smooth dashed curve. The dashed curve is also extended smoothly into the region beyond about 20 R_J where the electron density can be determined from the continuum radiation cutoff (See Figure 4).

For the Voyager 2 pass in Figure 9 a total of seven UHR events can be identified in the plasma wave data. These emissions are shown circled in the second panel from the top in Figure 9. As can be seen, these emissions are again well separated from the electrostatic emissions at $(3/2)f_g$ and $(5/2)f_g$. The electron densities determined from the upper hybrid resonance frequency are shown by the solid and open circles in the top panel. The solid circles are cases in which the UHR identification is considered unambiguous, and the open circles are cases in which the emissions could possibly be confused with bursts of narrow band kilometric radio emissions [*Kaiser and Desch*, 1980]. These electron densities have been shown by *Scudder et al.* [this issue] to be in good quantitative agreement with the electron densities measured by the Voyager plasma instrument. Also shown are the ion charge densities computed from the plasma (PLS) and low-energy charged particle (LECP) instruments. The charge density computed from the plasma instrument is the contribution due to positive ions, $N_e(\text{PLS}) = \sum Z_i N_i$, integrated over the energy range 10 eV to 6.0 keV [from *McNutt et al.*, this issue]. The charge density computed from the low-energy charged particle instrument is the contribution due to positive ions with energies greater than 30 keV, assuming that the plasma consists of doubly-charged oxygen [from *Krimigis et al.*, this issue], with $N_e(\text{LECP}) = 2N(O^{++})$. Although the charge state and ion

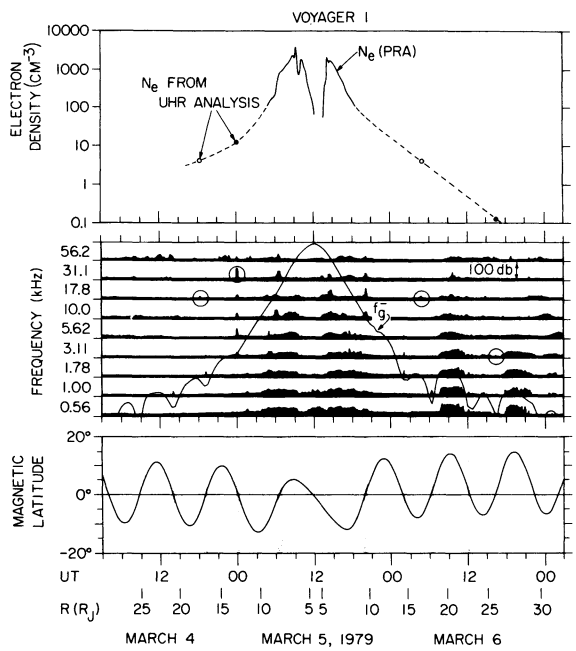

Fig. 8. The electron density near the Voyager 1 closest approach as obtained from upper hybrid emissions observed by the planetary radio astronomy (PRA) and plasma wave instruments. The most intense upper hybrid emissions (circled) always occur near crossings of the magnetic equator. The dashed line represents a smooth curve drawn through the available points and does not represent a continuous sequence of measurements.

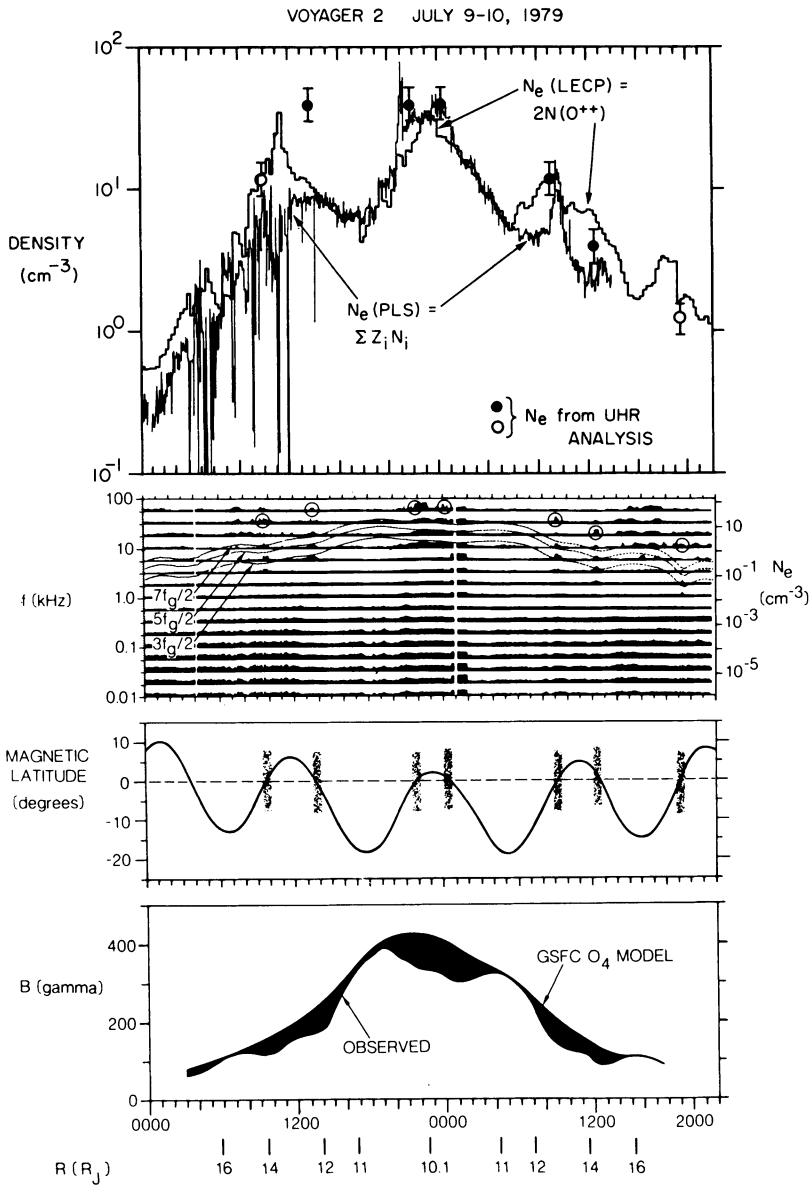

Fig. 9. The electron density near the Voyager 2 closest approach as obtained from upper hybrid emissions. All the upper hybrid emissions (circled) occurred at equator crossings. The solid dots represent very clear identifications, and the open dots represent cases where the UHR emissions may be confused with kilometric radio emission. The top panel also shows the electron density obtained from the low-energy charged particle (LECP) and from the plasma (PLS) instrument. The LECP measures ions with energies greater than 30 keV, and the PLS measures ions from 10 eV to 6 keV.

composition are not directly determined, the Voyager plasma measurements [*Bridge et al.*, 1979*a*, *b*] and extreme ultraviolet observations [*Broadfoot et al.*, 1979] provide substantial evidence for the presence of doubly-charged oxygen in the inner regions of the Jovian magnetosphere. Except for the gap in the ion density measurements between 6 and 30 keV, the total electron density should correspond approximately to the sum of the PLS and LECP densities. As can be seen, the sum of the electron densities computed from the PLS and LECP is in generally good quantitative agreement with the electron densities determined from the UHR emissions. The only significant exception is the UHR point at 1330 UT on July 9, which is well above both the PLS and LECP density curves. This point could be brought into acceptable agreement if a moderate (~50%) contribution to the total charge density occurred in the 6- to 30-keV energy gap between the two instruments. Also, as pointed out by *McNutt et al.* [this issue] and *Scudder et al.* [this issue], the contribution due to the LECP is subject to considerable uncertainty because of the difficulty in determining the composition. Unfortunately, because of the large error bars on the UHR electron density determination (plus or minus one-quarter of the channel spacing) it is not possible to provide a quantitatively meaningful test of the relative contributions of the PLS and LECP measurements to the total ion density.

A clearly defined 10-hour latitudinal modulation in both the PLS and LECP densities is evident in Figure 9, with the largest density occurring near the magnetic equator. Evidence of a corresponding modulation of the plasma pressure is also evident in the magnetic field data illustrated in the bottom panel of Figure 9, which shows strong depressions in the magnetic field strength in comparison with the Goddard Space

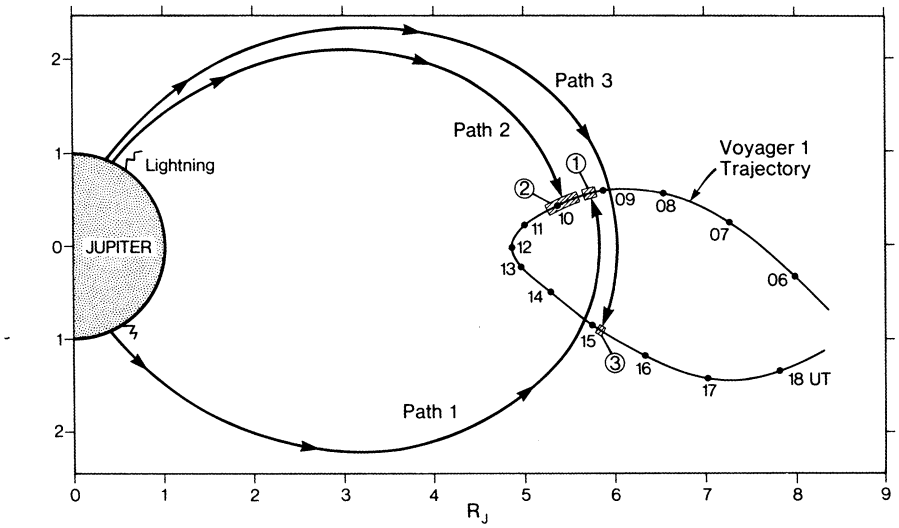

Fig. 10. Representative ray paths for three distinct groups of whistlers detected by Voyager 1. Paths 1 and 3 pass through the central region of the outer (hot) plasma torus, and path 1 passes through the low-density gap between the inner (cold) and outer (hot) regions of the torus.

Flight Center (GSFC) O4 model. This 10-hour modulation is not shown in the earlier preliminary analysis of the UHR electron density measurements by *Gurnett et al.* [1979*a*], since a smooth curve was drawn through the available UHR points. Note that all of the UHR events occur at the magnetic equator, near the peak in the 10-hour density modulation, thereby precluding any identification of this latitudinal effect from the UHR measurements. The strong magnetic field depressions near the magnetic equator indicate that the plasma pressure and temperature must be very large in this region. From the measured electron density the effective plasma temperature can be computed by equating the change in the magnetic field pressure to the plasma pressure, $\Delta(B^2/8\pi) = NKT$. Using values typical of the region near the closest approach, with $B = 400\ \gamma$, $\Delta B = 100\ \gamma$, $N_e = 38\ \text{cm}^{-3}$, and assuming that the pressure is mainly provided by doubly charged oxygen, with $N(O^{2+}) = (1/2)N_e$, the effective temperature is estimated to be about 9.2 keV. This very high temperature appears to be consistent with the fact that the PLS and LECP instruments give roughly comparable contributions to the total electron density in the region near closest approach (see Figure 9). Note, however, that the effective temperature computed above is the equivalent temperature for single Maxwellian velocity distribution. It is possible that the ion distribution function may be better represented by a two component Maxwellian consisting of hot and cold components. In this case the effective temperature determined above provides definite constraints on the densities and temperatures of the hot and cold components.

4. Electron Densities From Whistler Dispersions

Measurements of Whistler dispersions provide yet another method of determining properties of the electron density distribution in the Jovian magnetosphere. Whistlers, as is well known, are electromagnetic waves generated by lightning that are guided along the magnetic field from one hemisphere to the other at frequencies below the electron gyrofrequency. Because the velocity of propagation of the whistler mode depends on frequency, the arrival time of the lightning signal depends on frequency, thereby giving a characteristic whistling tone from which the name of this phenomena is derived. Since the propagation velocity also depends on the electron plasma frequency, the frequency dependence of the arrival time gives information on the electron density along the propagation path. Whistlers in fact provided the first definitive measurements of electron densities in the earth's magnetosphere [*Storey,* 1953]. For a review of the observations and theory of whistlers, see *Helliwell* [1965]. Since lightning generated whistlers have now been discovered by Voyager 1 at Jupiter [*Gurnett et al.,* 1979*b*], whistlers can be used to provide further information on the electron density distribution in the Jovian magnetosphere.

Because the dispersion of whistlers represents an integrated effect along the propagation path, whistlers do not provide a local determination of the electron density comparable to the measurements obtained from the continuum radiation and UHR emissions. Nevertheless, since the propagation path passes through regions of the magnetosphere that are not sampled by the local measurements, whistler dispersions provide a valuable constraint on the large scale electron density distribution. As shown by *Menietti and Gurnett* [1980], the whistler ray paths can to a good approximation be regarded as following the magnetic field line from the source of the lightning stroke to the spacecraft. Whistlers provide two essentially different types of information on the electron density distribution along the magnetic field line. First, because the whistler mode cannot propagate at frequencies above the electron plasma frequency [*Stix,* 1962], the upper frequency cutoff of a whistler provides a lower limit on the electron plasma frequency, hence electron density, at all points along the propagation path. Second, the dispersion of the whistler, which is determined by the arrival time t as a function of the frequency f, gives a weighted measure of the electron density along the

TABLE 4. Whistler Dispersions

Whistler Groups	Time, UT	R, R_J	Number of Whistlers	D, s $Hz^{1/2}$
Group 1	0912–0924	5.81–5.70	5	260 ± 25
Group 2	0932–1024	5.62–5.23	79	65 ± 20
Group 3	1506–1512	5.89–5.96	6	475 ± 50

The parameter D represents the average dispersion of the whistler.

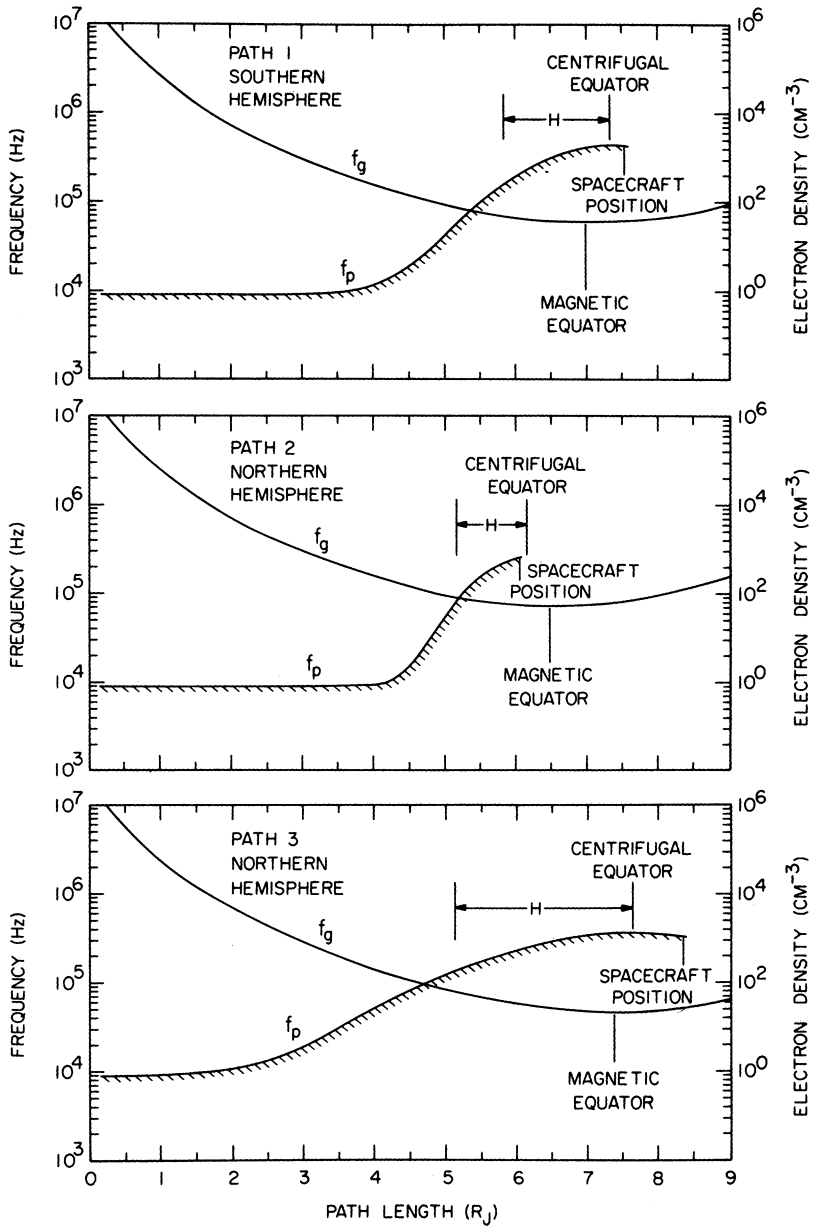

Fig. 11. Best fit electron density profiles computed for the three representative ray paths shown in Figure 10. The electron density profile in the torus is assumed to vary as $\exp[-(z/H)^2]$, where H is an effective scale height. The scale height H is adjusted to give the best fit to the average whistler dispersions along each path while constraining the electron density at the spacecraft to be in agreement with the local measurements of *Warwick et al.* [1979*a*].

propagation path. As shown by *Gurnett et al.* [1979*b*], the general equation for the travel time for parallel (field aligned) propagation is

$$t = \frac{1}{c}\int \left[1 + \frac{1}{2}\frac{f_p^2 f_g}{f(f_g - f)^2}\right] \Big/ \left[1 + \frac{f_p^2}{f(f_g - f)}\right]^{1/2} ds \qquad (1)$$

where the integration over ds is performed along the magnetic field line from the base of the ionosphere to the spacecraft. Examination of (1) shows that the primary contribution to the integral tends to occur near the equatorial plane where f_g is the smallest. If the plasma density is sufficiently high, i.e., if $f_p^2 \gg f f_g$, then (1) reduces to the following simple relation

$$t = \frac{D}{\sqrt{f}} \qquad D = \frac{1}{2c}\int \frac{f_p}{\sqrt{f_g}}\, ds \qquad (2)$$

where D is a parameter called the dispersion of the whistler. Equation (2) is valid for whistlers which have passed through the high-density regions of the Io plasma torus. Since f_g is nearly constant in the torus, the dispersion essentially gives the line integral of the square root of the electron density, $D \propto \int \sqrt{N'}\, ds$, integrated along the magnetic field line through the torus.

During the Voyager 1 pass by Jupiter a total of 167 whistlers were detected, 90 of which were suitable for dispersion measurements. The whistlers are not, however, uniformly distributed, but occur in three distinct groups, each with a characteristic dispersion. The regions where the three groups of whistlers were observed are shown by the crosshatched areas marked 1, 2, and 3 in Figure 10. Group 1 consists of five whistlers from about 0912 to 0924 UT, with dispersions ranging

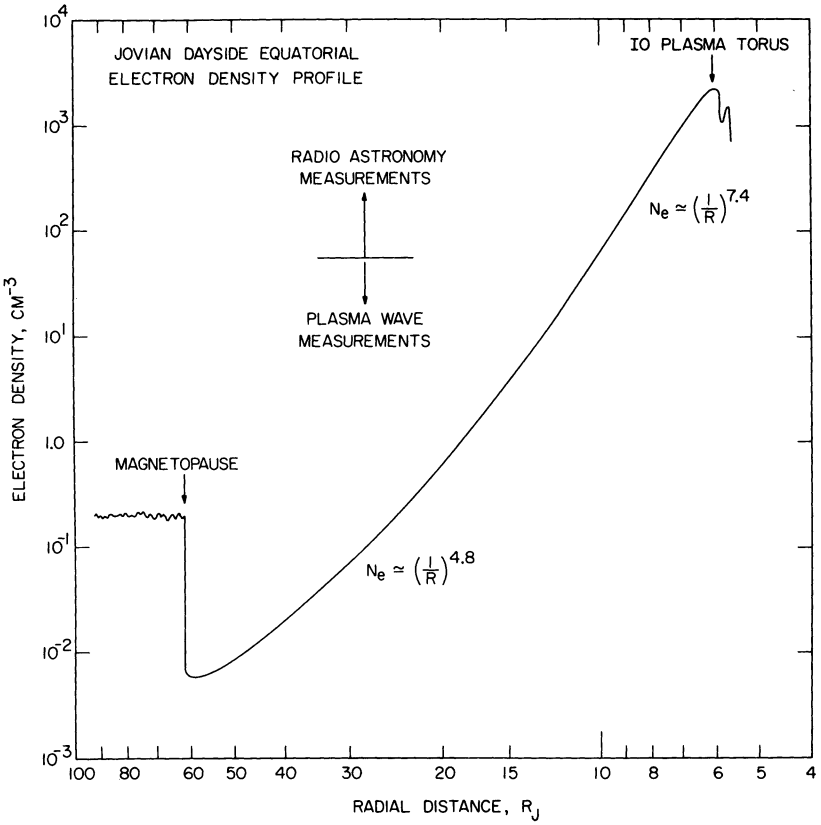

Fig. 12. A representative model of the dayside electron density profile near the magnetic equatorial plane based on a smooth best fit curve drawn through all of the inbound electron densities obtained from Voyager 1 and 2. Because of the large fluctuations, the actual electron density profile may deviate substantially from this best-fit curve.

from about 225 to 300 s $Hz^{1/2}$, group 2 consists of a large number (79) of whistlers from about 0932 to 1024 UT, with very low dispersions ranging from about 35 to 80 s $Hz^{1/2}$, and group 3 consists of six whistlers from about 1506 to 1512 UT, with dispersions ranging from about 390 to 570 s $Hz^{1/2}$. Because of the very large dispersions it is believed that groups 1 and 3 must have passed in opposite directions through the high density regions of the Io plasma torus along paths 1 and 3 as shown in Figure 10. The very low dispersion of group 2 on the other hand indicates that these whistlers could not have passed through the torus and must therefore have originated from lightning in the northern hemisphere, traveling along path 2 as shown in Figure 10. The basic characteristics of these three groups of whistlers are summarized in Table 4.

The extremely low dispersion of the whistlers following path 2 indicates that the electron density along this path must be very low. This path in fact appears to be located in the low-density gap between the inner (cold) and the outer (hot) regions of the plasma torus [*Bagenal et al.*, 1980]. Although a unique electron density profile cannot be obtained, a rough estimate can be made by assuming that the electron density is absolutely constant along this path. For the dispersions observed along path 2 the corresponding electron densities range from about 16.8 to 88 cm^{-3}. Actually, the average electron density must be lower than these values since some of the contribution to the dispersion must come from the torus. Since the whistler mode cannot propagate at frequencies above the electron plasma frequency, an absolute lower limit to the electron density at all points along path 2 can be obtained from the upper cutoff frequency of the whistlers, which in this region ranges up to about 6.5 kHz. The corresponding lower limit to the electron density at all points along the path is 0.52 cm^{-3}.

In order to proceed with a quantitative analysis of the whistler dispersion it is necessary to use a specific model for the electron density profile along the field line. Since most of the dispersion occurs because of propagation through the torus, we have adopted the centrifugal pressure balance model of the torus introduced by *Bagenal et al.* [1980]. In this model the density of each ion species is given by an equation of the form

$$N = N_0 \exp\left[-(z/H)^2\right] \tag{3}$$

where z is the distance along the magnetic field line from the centrifugal equator and H is an effective scale height. Since the electron density is given by a sum of terms of the form given by (3), we make the further assumption that the plasma is dominated by a single heavy ion. A single unique solution for the electron density profile can then be obtained by requiring that the electron density at the end of the propagation path match the local electron density measurements of *Warwick et al.* [1979*a*] and adjusting H to give the best fit to the observed dispersion. To assure that whistler propagation can occur along the field line outside the torus, a constant electron density of 1 cm^{-3} has been added to (3). This external background contribution is about the lowest density that would be consistent with the upper frequency cutoff of the observed whistlers. The best fits to the average dispersions listed in Table 4 for paths 1, 2, and 3 are shown in Figure 11. The best fit scale heights for paths 1 and 3, which pass directly through the torus, are $H_1 = 1.5\ R_J$ and $H_3 = 2.50\ R_J$. Since most of the

dispersion for these propagation paths occurs within the torus, these fits are almost totally insensitive to the background density outside of the torus and therefore give a very good determination of the effective scale height of the torus. For path 2, which just enters the outer edge of the torus, the corresponding best fit scale height is $H_2 = 0.9\ R_J$. This scale height is probably not very reliable because the propagation path does not sample the central region of the torus and because the very low dispersion makes the solution very sensitive to the choice of the background density outside of the torus.

5. CONCLUSION

In this paper we have presented a detailed analysis of the electron density distribution in the Jovian magnetosphere by using plasma wave measurements from Voyager 1 and 2. Three principal methods of determining the electron density were described, each with its own special advantages and limitations. The continuum radiation measurements provide the best measurements in the outer regions of the magnetosphere, beyond about 25 R_J, where the continuum radiation is most intense. The UHR measurements provide the best measurements in the inner regions of the magnetosphere, inside about 25 R_J, but have the disadvantage that these emissions usually occur only at the magnetic equator. The whistler measurements are confined to a small range of L shells inside of the Io plasma torus, but provide a unique capability to measure directly the effective scale height of the torus along these L shells. In all cases the electron density determinations are believed to be very accurate and reliable since the electron density determination is completely independent of spacecraft charging and sheath effects. The principal shortcoming at the present time is the limited amount of wideband data available for providing high-resolution measurements. As discussed by *Scarf et al.* [this issue], a large quantity of wideband data still remains to be processed and analyzed. When this processing is complete we expect to supplement the 16 channel survey plots presented in this paper with many more high resolution points, thereby giving added detail and resolution to the electron density measurements.

A semiquantitative model of the electron density profile determined from the plasma wave and radio astronomy instruments is shown in Figure 12. This profile is intended as a representative electron density profile through the central region of the dayside (inbound) plasma sheet and was obtained by drawing a smooth contour through all of the available wideband continuum radiation cutoffs and upper hybrid resonance frequencies measured by both Voyager 1 and 2. The magnetopause is shown at a typical radial distance and is not intended to correspond to any specific crossing. It is evident that the electron density increases smoothly with decreasing radial distance, reaching a well defined peak near the orbit of Io. No obvious sharp break or discontinuity is evident which could be identified as the outer boundary of the torus, consistent with the idea that the entire plasma distribution in the outer magnetosphere originates from plasma escaping radially outward from the Io plasma torus. Plotted on a log-log graph the power law index for the radial variation of the electron density, $N_e \propto (1/R)^\gamma$, varies from $\gamma = 7.4$ just outside of the torus to $\gamma = 4.8$ in the outer regions of the magnetosphere. Near closest approach whistler dispersion measurements have provided a direct determination of the scale height of the Io plasma torus. In the central region of the torus the effective scale height of the torus ranges from about 1.5 to 2.5 R_J. These scale heights appear to be somewhat larger than the heavy ion scale heights inferred from direct in situ measurements [*Bagenal et al.*, 1980; *Birmingham et al.*, this issue], which are on the order of 1 R_J or less. The larger effective scale height obtained from the whistler dispersion measurements is probably indicative of a substantial contribution from light ions (H^+, for example) in the region well away from the magnetic equator, which is not accessible to direct in situ measurements.

Acknowledgments. The authors express their thanks to S. M. Krimigis and H. Bridge for providing data for comparison in advance of publication and to F. Bagenal for comments and suggestions concerning the interpretation of the whistler dispersion measurements. The research at The University of Iowa was supported by NASA through contract 954013 with the Jet Propulsion Laboratory and through grants NGL-16-001-002 and NGL-16-001-043 with NASA Headquarters and by the Office of Naval Research. The research at TRW was supported by NASA through contract 954012 with the Jet Propulsion Laboratory.

REFERENCES

Ashour-Abdalla, M., C. F. Kennel, and W. Livesey, A parametric study of electron multiharmonic instabilities in the magnetosphere, *J. Geophys. Res., 84,* 6540, 1979.

Bagenal, F., J. D. Sullivan, and G. L. Siscoe, Spatial distribution of plasma in the Io torus, *Geophys. Res. Lett., 7,* 41, 1980.

Barbosa, D. D., Inverse Compton scattering due to magnetopause surface fluctuations in Jupiter's magnetospheric cavity, *Astrophys. J.,* in press, 1980.

Birmingham, T. J., J. K. Alexander, M. D. Desch, R. F. Hubbard, and B. M. Pedersen, Observations of electron gyroharmonic waves and the structure of the Io torus, *J. Geophys. Res.,* this issue.

Bridge, H. S., J. W. Belcher, A. J. Lazarus, J. D. Sullivan, R. L. McNutt, F. Bagenal, J. D. Scudder, E. C. Sittler, G. L. Siscoe, V. M. Vasyliunas, C. K. Goertz, and C. M. Yeates, Plasma observations near Jupiter: Initial results from Voyager 1, *Science, 204,* 987, 1979*a*.

Bridge, H. S., J. W. Belcher, A. J. Lazarus, J. D. Sullivan, F. Bagenal, R. L. McNutt, Jr., K. W. Ogilvie, J. D. Scudder, E. C. Sittler, V. M. Vasyliunas, and C. K. Goertz, Plasma observations near Jupiter: Initial results from Voyager 2, *Science, 206,* 972, 1979*b*.

Broadfoot, A. L., M. J. S. Belton, P. Z. Pakacs, B. R. Sandel, D. E. Shemansky, J. B. Holberg, J. M. Ajello, S. K. Atreya, T. M. Donahue, H. W. Moos, J. L. Bertaux, J. E. Blamont, D. F. Strobel, J. C. McConnel, A. Dalgarno, R. Goody, and M. B. McElroy, Extreme ultraviolet observations from Voyager 1 encounter with Jupiter, *Science, 204,* 979, 1979.

Christiansen, P. J., M. P. Gough, G. Martelli, J. J. Bloch, N. Cornilleau, J. Etcheto, R. Gendrin, C. Beghin, P. Decreau, and D. Jones, Geos-1 observations of electrostatic waves and their relationship with plasma parameters, *Space Sci. Rev., 22,* 383, 1978.

Frank, L. A., K. L. Ackerson, J. H. Wolfe, and J. D. Mihalov, Observations of plasmas in the Jovian magnetosphere, *J. Geophys. Res., 81,* 457, 1976.

Frankel, M. S., LF radio noise from the earth's magnetosphere, *Radio Sci., 8,* 991, 1973.

Gledhill, J. A., Magnetosphere of Jupiter, *Nature, 214,* 155, 1967.

Goertz, C. K., The Io-controlled decametric radiation, *Planet. Space Sci., 21,* 1431, 1973.

Gurnett, D. A., The earth as a radio source: The nonthermal continuum, *J. Geophys. Res., 80,* 2751, 1975.

Gurnett, D. A., and L. A. Frank, Thermal and suprathermal plasma densities in the outer magnetosphere, *J. Geophys. Res., 79,* 2355, 1974.

Gurnett, D. A., and L. A. Frank, Continuum radiation associated with low-energy electrons in the outer radiation zone, *J. Geophys. Res., 81,* 3875, 1976.

Gurnett, D. A., and R. R. Shaw, Electromagnetic radiation trapped in the magnetosphere above the plasma frequency, *J. Geophys. Res., 78,* 8136, 1973.

Gurnett, D. A., W. S. Kurth, and F. L. Scarf, Plasma wave observations near Jupiter: Initial results from Voyager 2, *Science, 206,* 987, 1979*a*.

Gurnett, D. A., R. R. Shaw, R. R. Anderson, and W. S. Kurth, Whistlers observed by Voyager 1: Detection of lightning on Jupiter, *Geophys. Res. Lett., 6,* 511, 1979*b*.

Gurnett, D. A., W. S. Kurth, and F. L. Scarf, The structure of the Jovian magnetotail from plasma wave observations, *Geophys. Res. Lett., 7,* 53, 1980.

Hartz, T. R., Low frequency noise emissions and their significance for energetic particle processes in the polar ionosphere, in *The Polar Ionosphere and Magnetospheric Processes,* p. 151, Gordon and Breach, New York, 1970.

Helliwell, R. A., *Whistlers and Related Ionospheric Phenomena,* p. 35, Stanford University Press, Stanford, Calif., 1965.

Hubbard, R. F., and T. J. Birmingham, Electrostatic emissions between electron gyroharmonics in the outer magnetosphere, *J. Geophys. Res., 83,* 4837, 1978.

Ioannidis, G., and N. Brice, Plasma densities in the Jovian magnetosphere: Plasma slingshot or Maxwell demon?, *Icarus, 14,* 360, 1971.

Jones, D., Source of terrestrial non-thermal radiation, *Nature, 260,* 686, 1976.

Kaiser, M. L., and M. D. Desch, Narrowband Jovian kilometric radiation: A new radio component, *Geophys. Res. Lett., 7,* 389, 1980.

Krimigis, S. M., T. P. Armstrong, W. I. Axford, C. O. Bostrom, C. Y. Fan, G. Gloeckler, L. J. Lanzerotti, E. P. Keath, R. D. Zwickl, J. F. Carbary, and D. C. Hamilton, Low-energy charged particle environment at Jupiter: A first look, *Science, 204,* 998, 1979*a*.

Krimigis, S. M., T. P. Armstrong, W. I. Axford, C. O. Bostrom, C. Y. Fan, G. Gloeckler, L. J. Lanzerotti, E. P. Keath, R. D. Zwickl, J. F. Carbary, and D. C. Hamilton, Hot plasma environment at Jupiter: Voyager 2 results, *Science, 206,* 977, 1979*b*.

Krimigis, S. M., J. F. Carbary, E. P. Keath, G. Gloeckler, W. I. Axford, L. J. Lanzerotti, and T. P. Armstrong, Characteristics of hot plasma in the Jovian magnetosphere, *J. Geophys. Res.,* this issue.

Kurth, W. S., J. D. Craven, L. A. Frank, and D. A. Gurnett, Intense electrostatic waves near the upper hybrid resonance frequency, *J. Geophys. Res., 84,* 4145, 1979.

Kurth, W. S., D. D. Barbosa, D. A. Gurnett, and F. L. Scarf, Electrostatic waves in the Jovian magnetosphere, *Geophys. Res. Lett., 7,* 57, 1980.

McNutt, R. L., J. W. Belcher, and H. S. Bridge, Positive ion observations in the middle magnetosphere of Jupiter, *J. Geophys. Res.,* this issue.

Melrose, D. B., A Theory for the nonthermal radio continuum in the terrestrial and Jovian magnetospheres, *J. Geophys. Res., 86,* 30, 1981.

Mendis, D. A., and W. I. Axford, Satellites and magnetospheres of the outer planets, *Ann. Rev. Earth Planet. Sci., 2,* 419, 1974.

Menietti, J. D., and D. A. Gurnett, Whistler propagation in the Jovian magnetosphere, *Geophys. Res. Lett., 7,* 49, 1980.

Michel, F. C., and P. A. Sturrock, Centrifugal instability of the Jovian magnetosphere and its interaction with the solar wind, *Planet. Space Sci., 22,* 1501, 1974.

Mosier, S. R., M. L. Kaiser, and L. W. Brown, Observations of noise bands associated with the upper hybrid resonance by the Imp 6 radio astronomy experiment, *J. Geophys. Res., 78,* 1673, 1973.

Rönnmark, K., H. Borg, P. J. Christiansen, M. P. Gough and D. Jones, Banded electron cyclotron harmonic instability—A first comparison of theory and experiment, *Space Sci. Rev., 22,* 401, 1978.

Scarf, F. L., and D. A. Gurnett, A plasma wave investigation for the Voyager mission, *Space Sci. Rev., 21,* 289, 1977.

Scarf, F. L., D. A. Gurnett, and W. S. Kurth, Jupiter plasma wave observations: An initial Voyager 1 overview, *Science, 204,* 991, 1979.

Scarf, F. L., D. A. Gurnett, and W. S. Kurth, Measurements of plasma wave spectra in Jupiter's magnetosphere, *J. Geophys. Res.,* this issue.

Scudder, J. D., E. C. Sittler, and H. S. Bridge, A survey of the plasma electron environment of Jupiter: A view from Voyager, *J. Geophys. Res.,* this issue.

Shaw, R. R., and D. A. Gurnett, Electrostatic noise bands associated with the electron gyrofrequency and plasma frequency in the outer magnetosphere, *J. Geophys. Res., 80,* 4259, 1975.

Shaw, R. R., and D. A. Gurnett, A test of two theories for the low frequency cutoffs of nonthermal continuum radiation, *J. Geophys. Res., 85,* 4571, 1980.

Stix, T. H., *The Theory of Plasma Waves,* p. 27, McGraw-Hill, New York, 1962.

Storey, L. R. O., An investigation of whistling atmospherics, *Phil. Trans. Royal Soc. London, Ser. A, 246,* 113, 1953.

Walsh, D., F. T. Haddock, and H. F. Schulte, Cosmic radio intensities at 1.225 and 2.0 Mc measured up to an altitude of 1700 km, *Space Res., 4,* 935, 1964.

Warwick, J. W., J. B. Pearce, A. C. Riddle, J. K. Alexander, M. D. Desch, M. L. Kaiser, J. R. Thieman, T. D. Carr, S. Gulkis, A. Boischot, C. C. Harvey, and B. M. Pedersen, Voyager 1 planetary radio astronomy observations near Jupiter, *Science, 204,* 995, 1979*a*.

Warwick, J. W., J. B. Pearce, A. C. Riddle, J. K. Alexander, M. D. Desch, M. L. Kaiser, J. R. Thieman, T. D. Carr, S. Gulkis, A. Boischot, Y. Leblanc, B. M. Pedersen, and D. H. Staelin, Planetary radio astronomy observations from Voyager 2 near Jupiter, *Science, 206,* 991, 1979*b*.

(Received June 12, 1980;
revised August 25, 1980;
accepted August 25, 1980.)